

# Escaping Local Minima with Quantum Coherent Cooling

Jia-Jin Feng(冯嘉进)<sup>1</sup> and Biao Wu(吴飙)<sup>1,2,3,\*</sup>

<sup>1</sup>*International Center for Quantum Materials, School of Physics, Peking University, Beijing 100871, China*

<sup>2</sup>*Wilczek Quantum Center, School of Physics and Astronomy,*

*Shanghai Jiao Tong University, Shanghai 200240, China*

<sup>3</sup>*Collaborative Innovation Center of Quantum Matter, Beijing 100871, China*

(Dated: February 22, 2023)

We propose a scheme to overcome the limitations of classical algorithms in finding global minima of cost functions. These algorithms are often trapped in local minima. Our approach utilizes quantum coherent cooling to facilitate coordinative tunneling through energy barriers in the encoded Hamiltonian system that represents the cost function. This is achieved by using a quantum coherent bath in the ground state as a heat sink to absorb energy from the system. Our proposed scheme can be implemented in the circuit quantum electrodynamics (cQED) system using a quantum cavity. We provide numerical evidence demonstrating quantum advantage in solving spin glass problems.

Optimization problems are prevalent in many areas where the global minima of cost functions represent the optimal solutions. Classical algorithms are usually able to quickly identify local minima but get trapped due to the complexity of the cost function. As a result, they are inefficient to find the global minima. This bottleneck is widely recognized in various fields, such as computational physics and machine learning.

Our proposed hybrid quantum-classical algorithm can address this problem. First, we use established classical techniques to identify a local minimum of the cost function for the given problem. We then encode the cost function as a Hamiltonian system, which is feasible for many problems [1–3]. The Hamiltonian system is coupled with a quantum coherent bath which has easy-to-prepare ground states and maintains coherence, facilitating coordinative quantum tunneling over high energy barriers. The quantum bath serves as both a heat sink and a means to escape the local minimum by tunneling into a lower value. This quantum coherent cooling approach is known as the quantum icebox algorithm (QIA) [4], which has been shown to achieve quantum advantage in

the unsorted search problem. The entire quantum-classical algorithm functions as a heterogeneous cooling process, where classical optimization is employed to find local minima, and quantum cooling helps to escape the local minima by tunneling through energy barriers. By alternating between classical optimization and quantum cooling, one can ultimately arrive at the global minimum. (See Fig. 1 for a visualization of this process.)

We specifically target a category of problems where the cost function involves  $n$  Boolean variables [5, 6], such as the 3-SAT problem and independent sets [7, 8]. In physical terms, these cost functions represent Hamiltonians of (pseudo-)spins [9, 10]. The configuration space for these problems consists of binary strings of zeros and ones (or  $\pm 1$  for spins), with each string representing a state  $\psi_s$ . Local minima for this class of problems are defined as states where neighboring states within one Hamming distance have higher cost function values (or energies). The Hamming distance is calculated by counting the number of different bits between two binary strings [11]. To solve these problems, our hybrid quantum-classical algorithm operates as follows (see also Fig. 1):

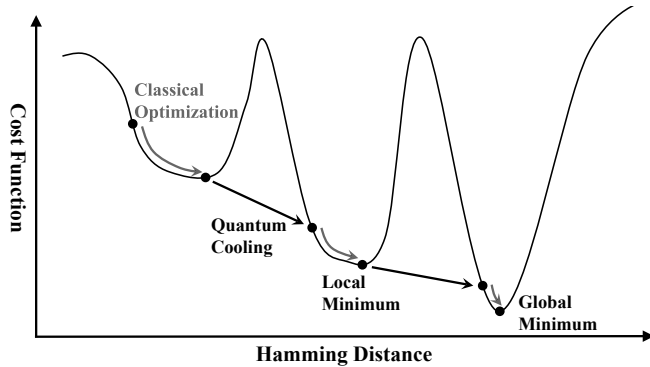


FIG. 1. The proposed heterogeneous cooling process.

1. Use arbitrary configuration  $\psi_{s0}$  as the initial condition to find out one of the local minima  $\psi_{s1}$  with classical algorithms.
2. Prepare the quantum state  $\psi_{s1}$  in the computational basis, denoted as  $|\psi_{s1}\rangle$ , and execute the QIA. Following quantum evolution, we obtain an entangled state  $|\Psi\rangle$ . We then proceed to measure the problem system in the computational basis, resulting in the random selection of a configuration denoted as  $\psi_{s2}$ .
3. Use the configuration  $\psi_{s2}$  as the initial condition to identify a different local minimum, represented as  $\psi_{s3}$ , using classical algorithms.
4. If  $\langle\psi_{s3}|H_s|\psi_{s3}\rangle \leq \langle\psi_{s1}|H_s|\psi_{s1}\rangle$ , then we update the initial configuration from  $\psi_{s1}$  to  $\psi_{s3}$ . In any case, we repeat the process starting from step 2.
5. Stop the iteration if  $\langle\psi_{s1}|H_s|\psi_{s1}\rangle$  is sufficiently small and no further update to  $\psi_{s1}$  is available.

\* [wubiao@pku.edu.cn](mailto:wubiao@pku.edu.cn)

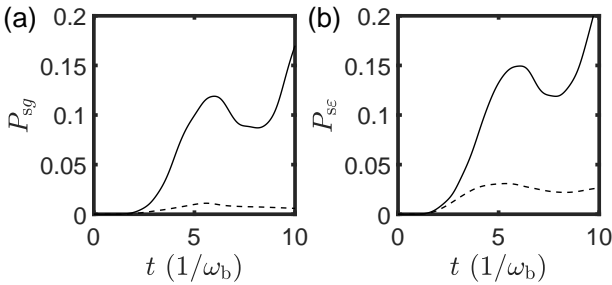


FIG. 2. Time evolution of the system cooled by the quantum bath (solid line) or the classical bath (dashed line). The number of qubits is  $n_s = 11$  ( $2^{-n_s} = 4.9 \times 10^{-4}$ ). The interaction strength is  $\lambda = 0.2\hbar\omega_b$ . The initial state of the problem system is the high energy local minimum. (a) The probability of the ground state of the problem system (global minimum). (b) The total probability of states of the problem system with lower on-site energy than the initial state.

The robustness of this hybrid quantum-classical algorithm to noise or errors is ensured by checking for mistakes in step 4 and by performing multiple rounds of optimization. The quantum acceleration in this algorithm is achieved in step 2, which employs the quantum bath for efficient cooling. We will demonstrate that the use of the quantum bath results in higher cooling efficiency.

Other hybrid quantum-classical algorithms [12–22] also combine classical and quantum methods as a compromise in the noisy intermediate-scale quantum (NISQ) era [23, 24], such as the variational quantum algorithm (VQA). In VQA, classical algorithms optimize the quantum gate parameters to reduce the number of quantum operations during the coherence time [25]. However, this approach faces challenges such as the barren plateau [16] and the need to avoid local minima. In our scheme, the classical algorithm only needs to optimize the initial state and find local minima, which is less problematic.

Since classical algorithms are well-established, let us now focus our attention to the quantum component. We will compare the cooling efficiency of the quantum coherence bath with the classical bath, specifically in the context of spin glasses. Spin glasses are typically difficult to cool down as they often have numerous local minima. Our numerical calculations show that the quantum coherence bath has a faster cooling speed and higher success rate in cooling compared to the classical bath (see Fig. 2).

To achieve cooling, ancilla interacting qubits are commonly used as the quantum bath [4, 26–28]. However, this approach often requires at least twice the number of qubits [4, 26], and maintaining entanglement among a large number of qubits is difficult in the NISQ era [23, 24]. As an alternative, we use a coherent cavity as the quantum bath, which is more feasible than using hundreds of qubits. The cavity is typically used in experiments to propagate interactions [29, 30] or measure states [31], and can take the form of a laser cavity [32, 33], inductor-capacitor ( $LC$ ) oscillator [31], or nanomechanical resonator [34].

Our discussion will focus on the circuit quantum electro-

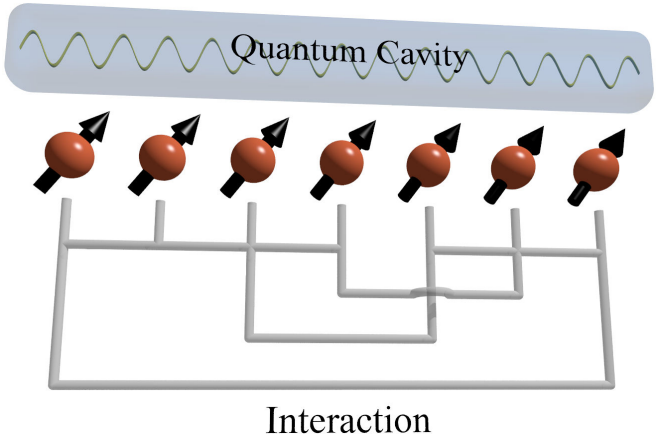


FIG. 3. (color online) The setup of our system. The coupled qubits encode the cost function and the quantum cavity serves as the bath.

dynamics (cQED) systems [31], although our algorithm can also be applied to other systems. The basic setup is depicted in Fig. 3, where the cavity in the superconductor circuit can be modeled as an  $LC$  oscillator. The angular frequency of the oscillator is given by  $\omega_b = 1/\sqrt{LC}$ , where  $L$  is the inductance and  $C$  is the capacitance. The quantum cavity acts as the bath, and its Hamiltonian is

$$H_b = \hbar\omega_b \left( \hat{b}^\dagger \hat{b} + \frac{1}{2} \right), \quad (1)$$

where  $\hat{b}^\dagger$  is the creator of the harmonic mode of the bath.

The qubits in Josephson junctions store the problem data, and their interactions are established through circuit connections. The Hamiltonian encoding the problem of  $n_s$  qubits is given by [3, 35–38]

$$H_s = \sum_{m=0}^{n_s-1} J_m^{(1)} \hat{\sigma}_m^z + \sum_{\langle m, m' \rangle} J_{m,m'}^{(2)} \hat{\sigma}_m^z \hat{\sigma}_{m'}^z, \quad (2)$$

which describes a spin glass that is difficult to cool down. The on-site energy is denoted by  $J_m^{(1)}$ , while  $J_{m,m'}^{(2)}$  represents the interaction between two qubits. This interaction can be spatially non-local, making the optimization problem more challenging. To facilitate quantum transitions,  $J_m^{(1)}$  and  $J_{m,m'}^{(2)}$  are multiples of  $\omega_b/2$ . The initial state of the system is a high-energy local minimum obtained from a classical algorithm. The qubits are part of cQED system, as shown in Fig. 3.

The interaction between the qubits and the cavity in the lumped-element circuit without spatial dependence is given by [31, 39–41]

$$H_\lambda = \lambda (\hat{b}^\dagger - \hat{b}) \sum_{m=0}^{n_s-1} (\hat{\sigma}_m^+ - \hat{\sigma}_m^-), \quad (3)$$

where  $\lambda$  is the interaction strength proportional to the capacitance. The interconnected capacitor introduces additional on-site capacitance, which can be absorbed in the parameters of  $H_s$  and  $H_b$ . Our scheme involves that  $\langle H_\lambda \rangle$  is comparable to

$\langle H_s \rangle$ , resulting in acceleration and novel phenomena beyond perturbation approach, including rotating wave approximation (RWA) [42–44].

The cooling process is governed by the fixed total Hamiltonian  $H = H_s + H_b + H_\lambda$  with little additional control. The circuit diagram is available in Appendix A. The total parity conservation  $e^{i\pi(b^\dagger b + 0.5\sum_{m=0}^{n_s-1} \hat{\sigma}_m^z)}$  can slightly simplify the numerical simulation.

The initial state of the bath is its ground state [45, 46], and the initial state of the problem system is set to be one of the high energy local minima of  $H_s$  in the  $\sigma_z$ -basis. Subsequently, the interaction  $H_\lambda$  is turned on, and the state evolves according to the Schrödinger equation. The energy of the system is absorbed by the bath through quantum tunneling, leading to the transfer of the system's state to other local minima with lower energy.

For comparison, we treat the cavity as a classical system by defining the generalized momentum  $\hat{Q}_b = i\sqrt{\hbar\omega_b C/2}(\hat{b}^\dagger - \hat{b})$  and the generalized position  $\hat{\Phi}_b = \sqrt{\hbar/2\omega_b C}(\hat{b}^\dagger + \hat{b})$  [31]. If the decoherence is strong, we can treat them as classical variables  $Q$  and  $\Phi$  [47–50]. The Hamiltonians for the bath in Eq. (1) and the interaction in Eq. (3) can be rewritten, respectively, as

$$H_b = \frac{Q_b^2}{2C_b} + \frac{\Phi_b^2}{2L_b}, \quad (4)$$

and

$$H_\lambda = \sqrt{\frac{2}{\hbar\omega_b C_b}}\lambda Q_b \sum_{m=0}^{n_s-1} \hat{\sigma}_m^y. \quad (5)$$

With the canonical equations  $\partial Q_b/\partial t = \partial \langle H \rangle / \partial \Phi_b$  and  $\partial \Phi_b/\partial t = \partial \langle H \rangle / \partial Q_b$  [51], we derive the total dynamical equations as

$$i\hbar \frac{\partial |\psi_s\rangle}{\partial t} = \left( H_s + \sqrt{\frac{2}{\hbar\omega_b C_b}}\lambda Q_b \sum_{m=0}^{n_s-1} \hat{\sigma}_m^y \right) |\psi_s\rangle, \quad (6)$$

$$\frac{\partial Q_b}{\partial t} = -\frac{\Phi_b}{L_b}, \quad (7)$$

$$\frac{\partial \Phi_b}{\partial t} = \frac{Q_b}{C_b} + \sqrt{\frac{2}{\hbar\omega_b C_b}}\lambda \sum_{m=0}^{n_s-1} \langle \hat{\sigma}_m^y \rangle. \quad (8)$$

Notice that  $Q_b = \Phi_b = 0$  is the fix point if all the qubits are aligned in the  $\sigma_z$  direction. The classical bath can be treated as a classical probability ensemble. For a fair comparison, the initial state of  $Q_b$  and  $\Phi_b$  is set to have the same probability distribution as the quantum ground state, which is  $\rho_c = e^{-(\Phi_b^2 + Q_b^2)/\pi}$  with  $q_b = Q_b/\sqrt{2\hbar\omega_b C_b}$  and  $\phi_b = \Phi_b\sqrt{\omega_b C_b/(2\hbar)}$  [48, 49]. The expectation value is considered as the independent average of all the evolution paths, i.e.,  $A = \int a * \rho_c d\phi_b d\Phi_b$ , where  $a$  is the observable for one initial condition and  $A$  is the expectation value.

No entanglement exists between the classical bath and the system, and the initial state of the bath  $\rho_c$  can be regarded as a mixed state. Throughout the evolution, the formation of entanglement is prohibited, and the total system remains in

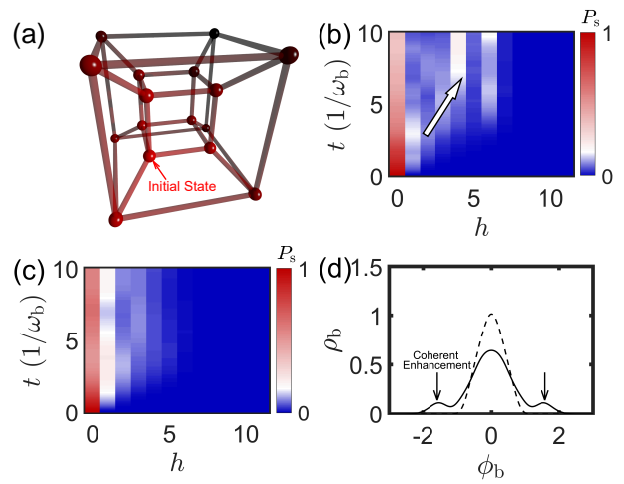


FIG. 4. (color online) (a) The hypercube where each vertex represents an eigenstate of the spin glass. The system is initially at the light red point, which is one of the local minima. The time evolution of the probability distribution as the problem system is cooled by (b) the quantum bath and (c) the classical bath.  $h$  is the Hamming distance from the initial state; the value at each  $h$  is the addition of probabilities of different states with the same  $h$ . (d) The probability distribution of the quantum bath (solid line) and the classical bath (dashed line) at  $t = 6/\omega_b$ . The parameters used in the numerical computation are the same as those in Fig. 2.

the product state  $|\psi_s\rangle \otimes |Q, \Phi\rangle$ . Moreover, some high energy paths of the classical bath are also not allowed, even though they could help the problem system surmount barriers. The numerical results depicted in Fig. 2 demonstrate that the classical bath performs worse than its quantum counterpart.

We simulate a system Hamiltonian with two local minima using Eq. (2). The initial state of the problem system is at the higher local minimum, while the bath is in its ground state. The Hamming distance between the local minima is  $\lceil n_s/2 \rceil$ , which increases the problem complexity. Cooling with the quantum bath does not always outperform the classical bath, but quantum resonance can strongly accelerate cooling when  $\lambda$  is tuned suitably [52]. Fig. 2 shows the probability  $P_g$  of the ground state changing with time. Cooling with the classical bath shows a modest increase over time, while the curve for the quantum bath shows a sharp increase due to quantum coherent enhancement. Our QIA cooling scheme has an advantage in escaping local minima.

This quantum acceleration is related to the entanglement and correlation numerically calculated in Appendix B. In the continuous variable system, we also find a similar quantum acceleration (see Appendix C).

The eigenstates of the spin glass problem system  $H_s$  are represented by a hypercube whose vertices correspond to the eigenstates in the  $\sigma_z$  basis as shown in Fig. 4(a). When the interaction is turned on, the wave function diffuses in the hypercube. As depicted in Fig. 4(b), the diffusion during quantum cooling is complex with peaks at the diffusion fronts, enabling faster reaching of the answers similar to diffusion in quantum

walks (QWs) [52–54]. On the other hand, the diffusion during classical cooling is weaker, and the probability distribution decreases monotonically with Hamming distance like the classical random walk (RW). These observations are depicted in Fig. 4(c).

Diffusion also occurs in the bath, leading to its state being driven away from its energy minimum. Better cooling performance is achieved when the bath is excited to higher energy states with greater probability and speed. Fig. 4(d) shows that the diffusion of the quantum bath is stronger with two peaks at the diffusion fronts, similar to the QW. On the other hand, the diffusion of the classical bath is weaker with monotonically decreasing fronts, as shown in Fig. 4(d). The classical bath diffuses very little without quantum coherence.

The diffusion in quantum cooling is similar to QW, as shown by the numerical results. To further illustrate this similarity, we consider a one qubit system with  $H_s = \hbar\omega_s \hat{\sigma}_z/2$  and  $\omega_s = \omega_b = \omega$ . It is the Jaynes–Cummings model of non-rotating wave form [31]. There are analytical results in the regime that one of the parameters  $\lambda$ ,  $\hbar\omega_s$  or  $\hbar\omega_b$  is much smaller than the others [55]. The non-perturbative resonant regime  $\lambda \sim \hbar\omega_s = \hbar\omega_b$  has rare analytical results. When the interaction is strong enough, an effective QW is observed in the dynamics. For a small time interval  $\Delta t$ , its unitary evolution is (see Appendix D for derivation) [56]

$$U = e^{-i\frac{H\Delta t}{\hbar}} = e^{-i\frac{H_0\Delta t}{\hbar}} U_p U_H + O(\Delta t^3), \quad (9)$$

where the on-site energy is  $H_0 = H_s + H_b$ . For a typical Hadamard walk in a one-dimensional space with a coin qubit, its unitary operation of each iteration is  $U_{\text{QW}} = U_p U_H$ , where  $U_H$  is the Hadamard gate to the coin qubit and  $U_p = e^{-i\hat{\sigma}_z' \Delta x \partial/\partial x}$  is the conditional walking operator controlled by the coin qubit. Therefore, in comparison, our system has an additional punishment term  $e^{-i\frac{H_0\Delta t}{\hbar}}$  that may disturb the phase [52]. However, this punishment term disappears when the eigenstates of  $H_0$  involved in the evolution are degenerate. This is exactly the case that we have studied where  $H_s$  and  $H_b$  are in resonance with matching energy gaps. It is well known that the average walking distance of RW is proportional to the square root of time  $\Delta x \sim \sqrt{t}$  while that of QW is proportional to the time  $\Delta x \sim t$  [54, 57]. The constructive interference makes QW diffuse faster than RW. It is also known that the entanglement between the coin qubit and the walking space is strong.

For the QW with multiple coin qubits, the situation is more complex (Appendix D). The analytical results always require non-local operation, such as the Grover's coin [58]. However, in our physical model, all the interactions are two-local. The numerical results in Fig. 4 suggests that QW still makes contribution in this complex case.

The concept of using a cavity for cooling has similarities to the quantum-circuit refrigerator (QCR) [59–61], utilizes an open cavity to cool a system. However, the QCR has strong dissipation in the cavity, and some schemes use a dissipative qubit as the bath [62, 63]. Although an open bath can introduce steady energy loss, the lack of quantum coherence may slow down cooling. Recent research suggests that the non-

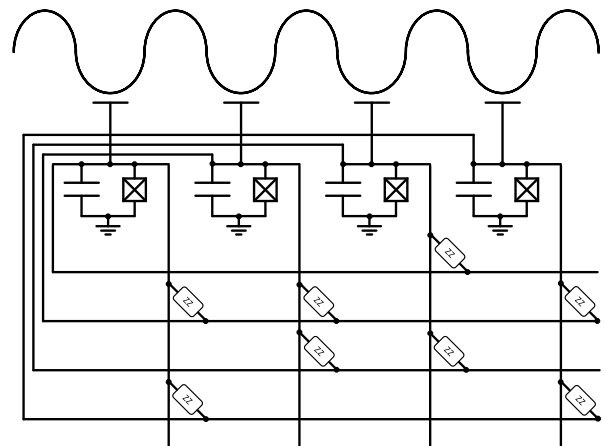


FIG. 5. The superconductor circuit of coherence cooling with the cavity. The long curve on the top is the cavity modeled by the LC oscillator. The symbol with a cross inside the square is the Josephson junction, which constitute the qubit with the parallel capacitor. There is no connection of each intersection between wires without a dot.

Markovian baths could improve the performance of a quantum refrigerator [64, 65]. In Appendix E, we show that the dissipation in the quantum bath will slow down the cooling speed.

In conclusion, we proposed a hybrid quantum-classical algorithm of coherent cooling to address the issue of local minima. It encodes the cost function in a superconductor circuit cooled by a quantum cavity, which outperforms a classical cavity due to the coordinative tunneling effect. Our results suggest that the faster diffusion of QW over classical RW is the underlying physics of this quantum speed-up. While we have focused on discrete variable problems, our scheme can be extended to continuous variable problems.

#### Appendix A: Superconductor Circuit of Coherent Cooling

Superconductor circuits can be utilized to physically implement the quantum icebox algorithm, and we can use the simplest charge qubits of Josephson junction as an example as shown in Fig. 5. Other types of qubits require slight modifications. For phase qubits, an additional injected current is needed for each qubit. For flux qubits, the on-site capacitors are replaced by inductors, and the interconnected capacitors are replaced by mutual inductors [36, 66, 67]. The on-site energy  $J_m^{(1)}$  can be tuned by the parallel capacitance of each qubit, while the interaction  $J_{m,m'}^{(2)}$  depends on the connectivity and coupling strength of the circuit matrix. The ZZ interaction is usually achieved by effective indirect interaction [35, 36, 68]. If the coherence of long-distance interaction is poor, indirect interaction can be used to improve it [29, 30, 69–72]. The crosstalk can be suppressed by a thick insulating layer made of high dielectric constant materials [71].

The design shown in Fig. 5 is inspired by the matrix circuit,

a technique commonly used in classical circuits for devices like screens, keyboards, and memories. The information is encoded in the intersections of the rows and columns, and only two circuit layers are needed, compared to the tens of layers used in modern classical CPUs.

## Appendix B: The Influence of Strong Interaction

For quantum acceleration, strong interaction is required to overcome localization, which typically occurs in low-symmetry quantum systems and suppresses the propagation of wave functions [73, 74].

We begin by examining the eigenstates of the total Hamiltonian  $H = H_s + H_b + H_\lambda$ . In the absence of interaction ( $H_\lambda = 0$ ), the eigenstates are product states of the system and bath. The system is fully localized at the vertex of the hypercube in the  $\sigma_z$  basis, with no nearby probability distribution. If localization decreases, probability distribution appears nearby, and the peak of probability  $P_{\max}$  decreases as the probability is shared with other states. Thus, localization strength can be determined by  $P_{\max}$  of eigenstates with low energy, shown in Fig. 6(a). Weak interaction ( $\lambda$ ) results in highly localized eigenstates [74], as seen on the left side of Fig. 6(a), where the wave function is unable to reach the whole Hilbert space, preventing solution discovery. On the other hand, Strong interaction causes delocalization [52, 75, 76], as shown on the right side of Fig. 6(a), with sufficient probability distribution around the ground state.

Furthermore, the degree of localization can also impact the strength of revivals. Revivals typically occur in (pseudo-)integrable systems, where the state after evolution partially returns to its initial state. When the interaction is weak, only a few states are involved, resulting in strong revivals as illustrated by the dashed line in Fig. 6(b). On the other hand, when the interaction is comparable to the on-site energy, more states are involved, leading to a rich energy spectrum of the initial state, and weaker revivals as shown by the solid line in Fig. 6(b).

We use the entanglement entropy and correlation to further investigate the quantum coherence between the quantum bath and the problem system. The entanglement entropy is given by

$$S = -\text{Tr}(\rho_s \ln \rho_s), \quad (\text{B1})$$

where  $\rho_s = \text{Tr}_b(\rho)$  is the reduced density matrix of the problem system. The entanglement entropy is shown in Fig. 6(c). The correlation can be described by the joint probability defined as [77]

$$\begin{aligned} C &= \langle \hat{P}_{\text{sg}} (\hat{I} - \hat{P}_{\text{bg}}) \rangle - \langle \hat{P}_{\text{sg}} \rangle \langle \hat{I} - \hat{P}_{\text{bg}} \rangle \\ &= -\langle \hat{P}_{\text{sg}} \hat{P}_{\text{bg}} \rangle + \langle \hat{P}_{\text{sg}} \rangle \langle \hat{P}_{\text{bg}} \rangle. \end{aligned} \quad (\text{B2})$$

Fig. 6(d) shows the correlation.

When the interaction between the problem system and the bath is weak ( $\langle H_\lambda \rangle < \langle H_0 \rangle$ ), the bath's influence can be considered a perturbation. Thus, the composed system can be approximated as a product state of the problem system and the

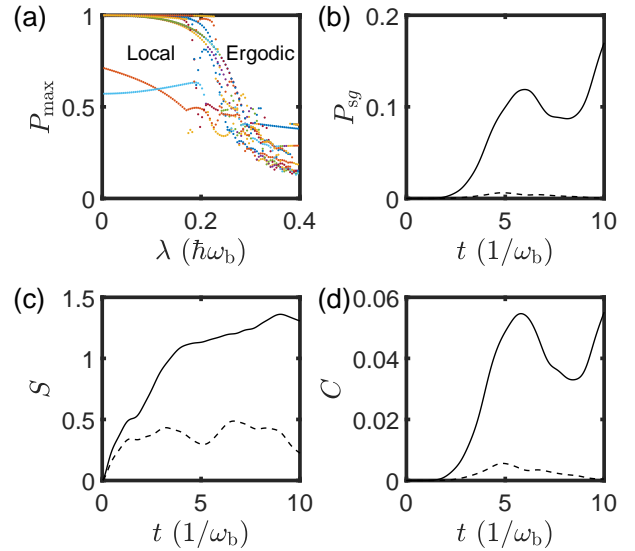


FIG. 6. (color online) (a) The localization strength of ten low energy eigenstates distinguished by different colors. Time dependent evolution of (b) the ground state probability of the problem system, (c) the entanglement entropy, and (d) the correlation of joint probability. The interaction strength is  $\lambda = 0.2\hbar\omega_b$  (solid line) and  $\lambda = 0.15\hbar\omega_b$  (dashed line).

bath, and the rotating wave approximation (RWA) holds to a large extent. Both the entanglement entropy and correlation are small, as shown by the dashed lines in Figure 6. In this scenario, the localization is strong, but the cooling efficiency is low [74].

As the interaction strength becomes comparable with the on-site energy,  $\langle H_\lambda \rangle \sim \langle H_0 \rangle$ , the composed system undergoes a phase transition[78] and the wave function becomes delocalized and ergodic[75, 76]. The product state approximation of the problem system and the bath is no longer valid. The entanglement and correlation between them increase significantly as depicted by the solid lines in Fig. 6, while the entanglement between the system and the classical bath is absent.

At the extremely strong coupling regime, the interaction  $H_\lambda$  dominates the dynamics. Despite the strong entanglement and correlation, the information from the system with  $H \approx H_\lambda$  is limited. Consequently, the cooling effect will vanish, leading to a low success rate.

## Appendix C: Cooling the Continuous System

For problems with continuous dynamical variables, they can also be encoded in Hamiltonians, for example, by mapping the variables to the generalized positions  $\Phi_s$  of Josephson junctions. The cost function for such a problem can be encoded in a Hamiltonian like this:

$$H_s = \frac{(\hat{\Phi}_s - \Phi_{\text{ex}})^2}{2L_s} - E_J \cos \frac{2\pi\hat{\Phi}_s}{\Phi_0}, \quad (\text{C1})$$

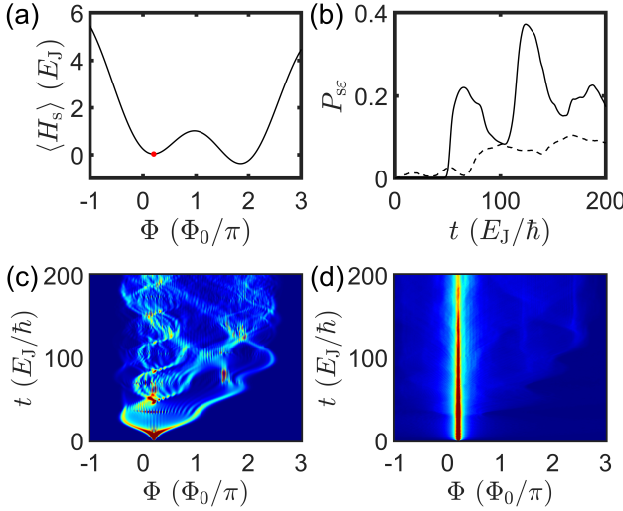


FIG. 7. (color online) (a) The system energy as a function of  $\Phi$ ; the red point indicates the initial state. (b) The time evolution of the total probability of the states which have lower on-site energy than the initial state. The solid line is for cooling using the quantum bath while the dashed line is cooling using the classical bath. (c) The time evolution of the probability distribution of the system with (c) the quantum bath (red for high values and blue for low) and (d) the classical bath.

where  $\Phi_{\text{ex}}$  is the external magnetic flux,  $\Phi_0$  is the quantum magnetic flux,  $L_s$  is the inductance, and  $E_J$  is the Josephson energy. These parameters can all be tuned [79]. The goal is to find the global minimum on  $\Phi_s$ , with the shape of the cost function shown in Fig. 7(a). The initial state is set at the higher local minimum.

The system-bath interaction can arise via the capacitor connection. This interaction can be described by the Hamiltonian

$$H_\lambda = -\frac{\hat{Q}_s \hat{Q}_b}{C_\lambda}, \quad (\text{C2})$$

where  $C_\lambda$  is the capacitance of the connection. The influence of the on-site capacitance has already been included in parameters of  $H_s$  and  $H_b$ .

Cooling process with the quantum bath satisfies the Schrödinger equation. Cooling process using the classical bath satisfies the following equations

$$i\hbar \frac{\partial |\psi_s\rangle}{\partial t} = \left( H_s - \frac{Q_b}{C_\lambda} \hat{Q}_s \right) |\psi_s\rangle, \quad (\text{C3})$$

$$\frac{\partial Q_b}{\partial t} = -\frac{\Phi_b}{L_b}, \quad (\text{C4})$$

$$\frac{\partial \Phi_b}{\partial t} = \frac{Q_b}{C_b} - \frac{\langle \hat{Q}_s \rangle}{C_\lambda}. \quad (\text{C5})$$

Comparing the time evolutions in Fig. 7(b), it is observed that the quantum bath yields better cooling efficiency than the classical bath in the continuous variable scenario. The quantum cooling displays characteristic quantum oscillations, while classical cooling is smoother. Fig. 7(c) illustrates the

coherent diffusion of quantum cooling through coordinative tunneling in the position space, displaying strong coherent enhancement at the wave function's fronts. Fig. 7(d) shows the smoother incoherent diffusion of classical cooling, with the strongest component trapped in the higher local minimum.

#### Appendix D: Quantum Walk Effect in the Coherent Cooling

Governed by the Schrödinger equation, the time evolution of the composed Hamiltonian can be divided into small steps

$$e^{-i\frac{H_t}{\hbar}} = \prod_{n=1}^{t/\Delta t} e^{-i\frac{H\Delta t}{\hbar}}. \quad (\text{D1})$$

The unitary operator for each step,  $U = e^{-i\frac{H\Delta t}{\hbar}}$  for the Hamiltonian in Eq.(9), can be approximated as [56]

$$\begin{aligned} U &= e^{-i\frac{\omega}{2} \hat{\sigma}_z \Delta t - i\omega (\hat{q}_b^2 + \hat{\phi}_b^2) \Delta t + i2\frac{\lambda}{\hbar} \hat{\sigma}_y \hat{q}_b \Delta t} \\ &\approx e^{-i\frac{\omega}{2} \hat{\sigma}_z \Delta t - i\omega (\hat{q}_b^2 + \hat{\phi}_b^2) \Delta t} e^{i2\frac{\lambda}{\hbar} \hat{\sigma}_y \hat{q}_b \Delta t} \\ &\quad e^{-\frac{1}{2} [-i\frac{\omega}{2} \hat{\sigma}_z \Delta t, i2\frac{\lambda}{\hbar} \hat{\sigma}_y \hat{q}_b \Delta t]} e^{-\frac{1}{2} [-i\omega (\hat{q}_b^2 + \hat{\phi}_b^2) \Delta t, i2\frac{\lambda}{\hbar} \hat{\sigma}_y \hat{q}_b \Delta t]} \\ &= e^{-i\frac{\omega}{2} \hat{\sigma}_z \Delta t - i\omega (\hat{q}_b^2 + \hat{\phi}_b^2) \Delta t} e^{i2\frac{\lambda}{\hbar} \hat{\sigma}_y \hat{q}_b \Delta t} e^{i\frac{\lambda}{\hbar} \omega \hat{\sigma}_x \hat{q}_b \Delta t^2} e^{-i\omega \frac{\lambda}{\hbar} \hat{\sigma}_y \hat{\phi}_b \Delta t^2} \\ &\approx e^{-i\frac{\omega}{2} \hat{\sigma}_z \Delta t - i\omega (\hat{q}_b^2 + \hat{\phi}_b^2) \Delta t} e^{i\frac{\lambda}{\hbar} (2\Delta t \hat{\sigma}_y + \omega \Delta t^2 \hat{\sigma}_x) \hat{q}_b} e^{-i\omega \frac{\lambda}{\hbar} \hat{\sigma}_y \hat{\phi}_b \Delta t^2}, \end{aligned} \quad (\text{D2})$$

where we have omitted all the  $O(\Delta t^3)$  terms. The dimensionless operator is  $\hat{q}_b = -i\partial/\partial\phi_b$ . Notice that the angle of rotation axis between  $U_p$  and  $U_H$  of the coin qubit is  $\pi/4$  in the Hadamard walk. In the time interval  $\Delta t = 2/\omega$ , this condition will be satisfied with

$$U = e^{-i\frac{H_0 \Delta t}{\hbar}} e^{-\frac{2\sqrt{2}\lambda}{\hbar\omega} \frac{\hat{\sigma}_y + \hat{\sigma}_x}{\sqrt{2}} \frac{\partial}{\partial\phi_b}} e^{-i\frac{4\lambda}{\hbar\omega} \hat{\sigma}_y \hat{\phi}_b}. \quad (\text{D3})$$

Then the rotation axis between the last two terms is also  $\pi/4$ . To simplify the comparison with the Hadamard walk, we do the transformation that

$$\begin{aligned} \hat{\sigma}_z &= \hat{\sigma}_x', \\ \hat{\sigma}_x &= \frac{\hat{\sigma}_z' - \hat{\sigma}_x'}{\sqrt{2}}, \\ \hat{\sigma}_y &= \frac{\hat{\sigma}_z' + \hat{\sigma}_x'}{\sqrt{2}}. \end{aligned} \quad (\text{D4})$$

Then the operation becomes

$$U = e^{-i\frac{H_0 \Delta t}{\hbar}} e^{-\hat{\sigma}_z' \frac{2\sqrt{2}\lambda}{\hbar\omega} \frac{\partial}{\partial\phi_b}} e^{i\frac{4\lambda}{\hbar\omega} \frac{\hat{\sigma}_z' + \hat{\sigma}_x'}{\sqrt{2}} \hat{\phi}_b}. \quad (\text{D5})$$

When  $4\lambda\phi_b/\hbar\omega = (2n+1)\pi$ , namely,  $\Delta\phi_b = \pi_0\hbar\omega/2\lambda$ , the last term is the Hadamard gate. Moreover, the displacement of conditional translation is  $\Delta\phi_b = 2\sqrt{2}\lambda/\hbar\omega$ , so the self-consistent requires  $\lambda = \sqrt{\pi}/2^{\frac{5}{4}}\hbar\omega$ . In summary, the unitary operation is

$$U = e^{-i\frac{H_0 \Delta t}{\hbar}} U_p U_H. \quad (\text{D6})$$

With the term  $e^{-i\frac{H_0 \Delta t}{\hbar}}$ , it is just the standard Hadamard walk.

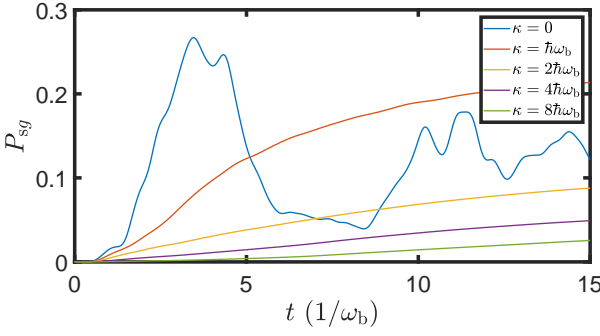


FIG. 8. (color online) The ground state probability of the problem system with different decoherence strength  $\kappa$  of the bath. Other parameters are  $n_s = 5$  and  $\lambda = 0.6\hbar\omega_b$ .

In the case of spin glass with multi-qubits, the operation is

$$U = e^{-i\frac{H_0\Delta t}{\hbar}} U_p U_H^{\otimes n_s}, \quad (\text{D7})$$

where the Hadamard gates require  $\omega_b \lambda \Delta \phi_b \Delta t^2 / \hbar = 2\pi$ . The conditional walker is more complex that

$$U_p = e^{i\frac{\lambda}{\hbar} \left( \sum_{m=1}^{n_s} \Delta t \hat{\sigma}_m^y + \sum_{m=1}^{n_s} J_m^{(1)} \Delta t^2 \hat{\sigma}_m^x + \sum_{\langle m, m' \rangle} J_{m, m'}^{(2)} \Delta t^2 (\hat{\sigma}_m^x \hat{\sigma}_{m'}^z + \hat{\sigma}_m^z \hat{\sigma}_{m'}^x) \right) \frac{\partial}{\partial \phi_b}} \quad (\text{D8})$$

#### Appendix E: Decoherence with Markov Master Equation

In the main text, we have discussed cooling with a coherent quantum bath using the Schrödinger equation. We now treat the cooling with the Markov master equation [80]

$$\frac{d\rho}{dt} = -\frac{i}{\hbar} [H, \rho] - \frac{\kappa}{\hbar} (b^\dagger b \rho + \rho b^\dagger b - 2b\rho b^\dagger), \quad (\text{E1})$$

where  $\kappa$  represents the decoherence strength of the bath. In Fig. 8, we compare the cooling processes with different values of  $\kappa$ . The case with  $\kappa = 0$  corresponds to the case discussed in the main text.

The numerical results indicate that the cooling process without decoherence is faster in the early stage. Although decoherence can extract energy from the bath irreversibly, it can disrupt the quantum acceleration by suppressing the off-diagonal terms of the density matrix  $\rho$ . This transition between quantum states requires these off-diagonal terms, and the present of decoherence can hinder quantum tunneling.

At the late cooling stage, the cooling process reaches saturation. Even a small amount of decoherence can decrease the revival from quantum oscillation [73, 81]. Strong decoherence, on the other hand, can entirely suppress the quantum transition.

We consider a simple case to demonstrate the effect of decoherence on quantum acceleration, where both the problem system and the bath are two-level systems [64, 65]. The

states  $|\sigma_z, n_b\rangle$  are re-defined as  $|2\rangle \equiv |1, 0\rangle$ ,  $|1\rangle \equiv |-1, 1\rangle$ , and  $|0\rangle \equiv |-1, 0\rangle$ . Eq. (E1) in RWA can then be written as

$$\frac{d\rho_{22}}{dt} = \frac{\lambda}{\hbar} (i\rho_{12} - i\rho_{21}), \quad (\text{E2})$$

$$\frac{d\rho_{12}}{dt} = \frac{\lambda}{\hbar} (i\rho_{22} - i\rho_{11}) - \frac{\kappa}{\hbar} \rho_{12}, \quad (\text{E3})$$

$$\frac{d\rho_{11}}{dt} = \frac{\lambda}{\hbar} (-i\rho_{12} + i\rho_{21}) - 2\frac{\kappa}{\hbar} \rho_{11}, \quad (\text{E4})$$

$$\frac{d\rho_{00}}{dt} = 2\frac{\kappa}{\hbar} \rho_{11}, \quad (\text{E5})$$

where  $\rho_{12}^\dagger = \rho_{21}$ . The initial condition is  $\rho_{22} = 1$  and other elements of the density matrix are zero. The solution is

$$\rho_{22} = e^{-\frac{\kappa t}{\hbar}} \left( \frac{1 + \cos 2\Omega t}{2} \frac{\lambda^2}{\hbar^2 \Omega^2} - \frac{\cos 2\Omega t}{4} \frac{\kappa^2}{\hbar^2 \Omega^2} + \frac{\sin 2\Omega t}{4} \frac{\kappa}{\hbar \Omega} \right), \quad (\text{E6})$$

where  $\hbar\Omega = \sqrt{\lambda^2 - \kappa^2/4}$  and  $P_{sg} = 1 - \rho_{22} = \rho_{11} + \rho_{00}$ . It is a damped oscillator with the decoherence  $\kappa$  slowing down the oscillation angular frequency from  $\lambda/\hbar$  to  $\Omega$ . As a result, the quantum transition between  $|2\rangle$  and  $|1\rangle$  is also slowed down.

(D8) When the decoherence is small  $\kappa \ll \lambda$ , the system is in the underdamped regime with oscillations. The probability of being in the ground state is approximately given by

$$P_{sg} \approx 1 - e^{-\frac{\kappa t}{\hbar}} \left( \frac{1 + \cos \frac{2\lambda t}{\hbar}}{2} + \frac{\kappa}{2\lambda} \sin \frac{2\lambda t}{\hbar} \right). \quad (\text{E7})$$

In the early stage  $t \ll \hbar/\lambda$ , Eq. (E7) can be simplified to

$$P_{sg} \approx \sin^2 \frac{\lambda t}{\hbar} - \frac{\lambda^2 \kappa}{2\hbar^3} t^3. \quad (\text{E8})$$

The last term is due to decoherence, and its negativity implies that it leads to deceleration.

When  $\kappa \gg \lambda$ , the system is in the overdamped regime without oscillations, and the ground state probability is given by

$$P_{sg} \approx 1 - e^{-\frac{2\lambda^2}{\hbar\kappa} t}, \quad (\text{E9})$$

which indicates that stronger decoherence leads to slower cooling. In this regime, the bath is almost frozen in its ground state, and the dynamics are essentially static.

For multi-qubits, as depicted in Fig. 8, there is also exponential behavior observed in the presence of strong dissipation, similar to Eq. (E9). Therefore, to ensure reasonable quantum acceleration, the decoherence strength should not greatly exceed the tunneling strength during quantum computing.

- 
- [1] E. Farhi, J. Goldstone, S. Gutmann, J. Lapan, A. Lundgren, and D. Preda, A quantum adiabatic evolution algorithm applied to random instances of an np-complete problem, *Science* **292**, 472 (2001).
- [2] E. Farhi, J. Goldstone, and S. Gutmann, Quantum adiabatic evolution algorithms versus simulated annealing (2002), [arXiv:quant-ph/0201031](https://arxiv.org/abs/quant-ph/0201031).
- [3] A. Lucas, Ising formulations of many np problems, *Frontiers in Physics* **2**, 10.3389/fphy.2014.00005 (2014).
- [4] J.-J. Feng, B. Wu, and F. Wilczek, Quantum computing by coherent cooling, *Phys. Rev. A* **105**, 052601 (2022).
- [5] B. Bollig and I. Wegener, Improving the variable ordering of obdds is np-complete, *IEEE Transactions on Computers* **45**, 993 (1996).
- [6] V. Kolmogorov and R. Zabin, What energy functions can be minimized via graph cuts?, *IEEE Transactions on Pattern Analysis and Machine Intelligence* **26**, 147 (2004).
- [7] C. A. Tovey, A simplified np-complete satisfiability problem, *Discrete Applied Mathematics* **8**, 85 (1984).
- [8] S. Sakai, M. Togasaki, and K. Yamazaki, A note on greedy algorithms for the maximum weighted independent set problem, *Discrete Applied Mathematics* **126**, 313 (2003).
- [9] Y. Hu, Z. Zhang, and B. Wu, Quantum algorithm for a set of quantum 2sat problems, *Chinese Physics B* **30**, 020308 (2021).
- [10] H. Yu, F. Wilczek, and B. Wu, Quantum algorithm for approximating maximum independent sets, *Chinese Physics Letters* **38**, 030304 (2021).
- [11] C. A. Trugenberger, Probabilistic quantum memories, *Phys. Rev. Lett.* **87**, 067901 (2001).
- [12] E. Farhi, J. Goldstone, and S. Gutmann, A quantum approximate optimization algorithm (2014), [arXiv:1411.4028 \[quant-ph\]](https://arxiv.org/abs/1411.4028).
- [13] A. Peruzzo, J. McClean, P. Shadbolt, M.-H. Yung, X.-Q. Zhou, P. J. Love, A. Aspuru-Guzik, and J. L. O'Brien, A variational eigenvalue solver on a photonic quantum processor, *Nature Communications* **5**, 4213 (2014).
- [14] J. R. McClean, J. Romero, R. Babbush, and A. Aspuru-Guzik, The theory of variational hybrid quantum-classical algorithms, *New Journal of Physics* **18**, 023023 (2016).
- [15] J. I. Colless, V. V. Ramasesh, D. Dahmen, M. S. Blok, M. E. Kimchi-Schwartz, J. R. McClean, J. Carter, W. A. de Jong, and I. Siddiqi, Computation of molecular spectra on a quantum processor with an error-resilient algorithm, *Phys. Rev. X* **8**, 011021 (2018).
- [16] J. R. McClean, S. Boixo, V. N. Smelyanskiy, R. Babbush, and H. Neven, Barren plateaus in quantum neural network training landscapes, *Nature Communications* **9**, 4812 (2018).
- [17] S. McArdle, T. Jones, S. Endo, Y. Li, S. C. Benjamin, and X. Yuan, Variational ansatz-based quantum simulation of imaginary time evolution, *npj Quantum Information* **5**, 75 (2019).
- [18] L. Zhou, S.-T. Wang, S. Choi, H. Pichler, and M. D. Lukin, Quantum approximate optimization algorithm: Performance, mechanism, and implementation on near-term devices, *Phys. Rev. X* **10**, 021067 (2020).
- [19] M. Cerezo, A. Sone, T. Volkoff, L. Cincio, and P. J. Coles, Cost function dependent barren plateaus in shallow parametrized quantum circuits, *Nature Communications* **12**, 1791 (2021).
- [20] S. Endo, Z. Cai, S. C. Benjamin, and X. Yuan, Hybrid quantum-classical algorithms and quantum error mitigation, *Journal of the Physical Society of Japan* **90**, 032001 (2021).
- [21] T. Xin, L. Che, C. Xi, A. Singh, X. Nie, J. Li, Y. Dong, and D. Lu, Experimental quantum principal component analysis via parametrized quantum circuits, *Phys. Rev. Lett.* **126**, 110502 (2021).
- [22] Z.-D. Wang, P.-L. Zheng, B. Wu, and Y. Zhang, Quantum dropout for efficient quantum approximate optimization algorithm on combinatorial optimization problems (2022), [arXiv:2203.10101 \[quant-ph\]](https://arxiv.org/abs/2203.10101).
- [23] J. Preskill, Quantum Computing in the NISQ era and beyond, *Quantum* **2**, 79 (2018).
- [24] K. Bharti, A. Cervera-Lierta, T. H. Kyaw, T. Haug, S. Alperin-Lea, A. Anand, M. Degroote, H. Heimonen, J. S. Kottmann, T. Menke, W.-K. Mok, S. Sim, L.-C. Kwek, and A. Aspuru-Guzik, Noisy intermediate-scale quantum algorithms, *Rev. Mod. Phys.* **94**, 015004 (2022).
- [25] Y. Cao, J. Romero, J. P. Olson, M. Degroote, P. D. Johnson, M. Kieferová, I. D. Kivlichan, T. Menke, B. Peropadre, N. P. D. Sawaya, S. Sim, L. Veis, and A. Aspuru-Guzik, Quantum chemistry in the age of quantum computing, *Chemical Reviews* **119**, 10856 (2019).
- [26] A. Matthes, M. Rudner, A. Rosch, and E. Berg, Programmable adiabatic demagnetization for systems with trivial and topological excitations (2022), [arXiv:2210.17256 \[quant-ph\]](https://arxiv.org/abs/2210.17256).
- [27] N. A. Rodríguez-Briones and R. Laflamme, Achievable polarization for heat-bath algorithmic cooling, *Phys. Rev. Lett.* **116**, 170501 (2016).
- [28] S. Zaiser, C. T. Cheung, S. Yang, D. B. R. Dasari, S. Raeisi, and J. Wrachtrup, Cyclic cooling of quantum systems at the saturation limit, *npj Quantum Information* **7**, 92 (2021).
- [29] J. Majer, J. M. Chow, J. M. Gambetta, J. Koch, B. R. Johnson, J. A. Schreier, L. Frunzio, D. I. Schuster, A. A. Houck, A. Wallraff, A. Blais, M. H. Devoret, S. M. Girvin, and R. J. Schoelkopf, Coupling superconducting qubits via a cavity bus, *Nature* **449**, 443 (2007).
- [30] A. Blais, J. Gambetta, A. Wallraff, D. I. Schuster, S. M. Girvin, M. H. Devoret, and R. J. Schoelkopf, Quantum-information processing with circuit quantum electrodynamics, *Phys. Rev. A* **75**, 032329 (2007).
- [31] A. Blais, A. L. Grimsmo, S. M. Girvin, and A. Wallraff, Circuit quantum electrodynamics, *Rev. Mod. Phys.* **93**, 025005 (2021).
- [32] G. Kurizki, P. Bertet, Y. Kubo, K. Mølmer, D. Petrosyan, P. Rabl, and J. Schmiedmayer, Quantum technologies with hybrid systems, *Proceedings of the National Academy of Sciences* **112**, 3866 (2015).
- [33] M. Aspelmeyer, T. J. Kippenberg, and F. Marquardt, Cavity optomechanics, *Rev. Mod. Phys.* **86**, 1391 (2014).
- [34] A. N. Cleland and M. R. Geller, Superconducting qubit storage and entanglement with nanomechanical resonators, *Phys. Rev. Lett.* **93**, 070501 (2004).
- [35] M. C. Collodo, J. Herrmann, N. Lacroix, C. K. Andersen, A. Remm, S. Lazar, J.-C. Besse, T. Walter, A. Wallraff, and C. Eichler, Implementation of conditional phase gates based on tunable  $zz$  interactions, *Phys. Rev. Lett.* **125**, 240502 (2020).
- [36] P. Zhao, P. Xu, D. Lan, J. Chu, X. Tan, H. Yu, and Y. Yu, High-contrast  $zz$  interaction using superconducting qubits with opposite-sign anharmonicity, *Phys. Rev. Lett.* **125**, 200503 (2020).
- [37] M. Gong, S. Wang, C. Zha, M.-C. Chen, H.-L. Huang, Y. Wu, Q. Zhu, Y. Zhao, S. Li, S. Guo, H. Qian, Y. Ye, F. Chen, C. Ying, J. Yu, D. Fan, D. Wu, H. Su, H. Deng, H. Rong, K. Zhang, S. Cao, J. Lin, Y. Xu, L. Sun, C. Guo, N. Li, F. Liang, V. M. Bastidas, K. Nemoto, W. J. Munro, Y.-H. Huo, C.-Y. Lu, C.-

- Z. Peng, X. Zhu, and J.-W. Pan, Quantum walks on a programmable two-dimensional 62-qubit superconducting processor, *Science* **372**, 948 (2021).
- [38] A. D. King, S. Suzuki, J. Raymond, A. Zucca, T. Lanting, F. Altomare, A. J. Berkley, S. Ejtemaei, E. Hoskinson, S. Huang, E. Ladizinsky, A. J. R. MacDonald, G. Marsden, T. Oh, G. Poulin-Lamarre, M. Reis, C. Rich, Y. Sato, J. D. Whittaker, J. Yao, R. Harris, D. A. Lidar, H. Nishimori, and M. H. Amin, Coherent quantum annealing in a programmable 2000 qubit ising chain, *Nature Physics* **18** (2022).
- [39] M. F. Gely, A. Parra-Rodriguez, D. Bothner, Y. M. Blanter, S. J. Bosman, E. Solano, and G. A. Steele, Convergence of the multi-mode quantum rabi model of circuit quantum electrodynamics, *Phys. Rev. B* **95**, 245115 (2017).
- [40] M. Malekakhlagh, A. Petrescu, and H. E. Türeci, Cutoff-free circuit quantum electrodynamics, *Phys. Rev. Lett.* **119**, 073601 (2017).
- [41] T. Miyanaga, A. Tomonaga, H. Ito, H. Mukai, and J. Tsai, Ultra-strong tunable coupler between superconducting *lc* resonators, *Phys. Rev. Applied* **16**, 064041 (2021).
- [42] R. Kuzmin, N. Mehta, N. Grabon, R. Mencia, and V. E. Manucharyan, Superstrong coupling in circuit quantum electrodynamics, *npj Quantum Information* **5**, 20 (2019).
- [43] P. Talkner and P. Hänggi, Colloquium: Statistical mechanics and thermodynamics at strong coupling: Quantum and classical, *Rev. Mod. Phys.* **92**, 041002 (2020).
- [44] J. Liu, K. A. Jung, and D. Segal, Periodically driven quantum thermal machines from warming up to limit cycle, *Phys. Rev. Lett.* **127**, 200602 (2021).
- [45] M. Um, J. Zhang, D. Lv, Y. Lu, S. An, J.-N. Zhang, H. Nha, M. S. Kim, and K. Kim, Phonon arithmetic in a trapped ion system, *Nature Communications* **7**, 11410 (2016).
- [46] D. I. Schuster, A. A. Houck, J. A. Schreier, A. Wallraff, J. M. Gambetta, A. Blais, L. Frunzio, J. Majer, B. Johnson, M. H. Devoret, S. M. Girvin, and R. J. Schoelkopf, Resolving photon number states in a superconducting circuit, *Nature* **445**, 515 (2007).
- [47] A. Caldeira and A. Leggett, Path integral approach to quantum brownian motion, *Physica A: Statistical Mechanics and its Applications* **121**, 587 (1983).
- [48] A. Polkovnikov, Phase space representation of quantum dynamics, *Annals of Physics* **325**, 1790 (2010).
- [49] T. L. Curtright and C. K. Zachos, Quantum mechanics in phase space, *Asia Pacific Physics Newsletter* **01**, 37 (2012).
- [50] Z. Wang, J. Feng, and B. Wu, Microscope for quantum dynamics with planck cell resolution, *Phys. Rev. Research* **3**, 033239 (2021).
- [51] Q. Zhang and B. Wu, General approach to quantum-classical hybrid systems and geometric forces, *Phys. Rev. Lett.* **97**, 190401 (2006).
- [52] A. M. Childs and J. Goldstone, Spatial search by quantum walk, *Phys. Rev. A* **70**, 022314 (2004).
- [53] A. M. Childs, Universal computation by quantum walk, *Phys. Rev. Lett.* **102**, 180501 (2009).
- [54] S. E. Venegas-Andraca, Quantum walks: a comprehensive review, *Quantum Information Processing* **11**, 1015 (2012).
- [55] J. Casanova, G. Romero, I. Lizuain, J. J. García-Ripoll, and E. Solano, Deep strong coupling regime of the jaynes-cummings model, *Phys. Rev. Lett.* **105**, 263603 (2010).
- [56] F. Casas, A. Murua, and M. Nadinic, Efficient computation of the zassenhaus formula, *Computer Physics Communications* **183**, 2386 (2012).
- [57] J. Kempe, Quantum random walks: An introductory overview, *Contemporary Physics* **44**, 307 (2003).
- [58] I. Carneiro, M. Loo, X. Xu, M. Girerd, V. Kendon, and P. L. Knight, Entanglement in coined quantum walks on regular graphs, *New Journal of Physics* **7**, 156 (2005).
- [59] K. Y. Tan, M. Partanen, R. E. Lake, J. Govenius, S. Masuda, and M. Möttönen, Quantum-circuit refrigerator, *Nat. Commun.* **8**, 15189 (2017).
- [60] M. Silveri, H. Grabert, S. Masuda, K. Y. Tan, and M. Möttönen, Theory of quantum-circuit refrigeration by photon-assisted electron tunneling, *Phys. Rev. B* **96**, 094524 (2017).
- [61] H. Hsu, M. Silveri, A. Gunyhó, J. Goetz, G. Catelani, and M. Möttönen, Tunable refrigerator for nonlinear quantum electric circuits, *Phys. Rev. B* **101**, 235422 (2020).
- [62] M. Raghunandan, F. Wolf, C. Ospelkaus, P. O. Schmidt, and H. Weimer, Initialization of quantum simulators by sympathetic cooling, *Science Advances* **6**, eaaw9268 (2020).
- [63] S. Polla, Y. Herasymenko, and T. E. O'Brien, Quantum digital cooling, *Phys. Rev. A* **104**, 012414 (2021).
- [64] P. A. Camati, J. F. G. Santos, and R. M. Serra, Employing non-markovian effects to improve the performance of a quantum otto refrigerator, *Phys. Rev. A* **102**, 012217 (2020).
- [65] Q. Zhang, Z.-X. Man, and Y.-J. Xia, Non-markovianity and the landauer principle in composite thermal environments, *Phys. Rev. A* **103**, 032201 (2021).
- [66] R. Harris, T. Lanting, A. J. Berkley, J. Johansson, M. W. Johnson, P. Bunyk, E. Ladizinsky, N. Ladizinsky, T. Oh, and S. Han, Compound josephson-junction coupler for flux qubits with minimal crosstalk, *Phys. Rev. B* **80**, 052506 (2009).
- [67] X. Dai, D. Tennant, R. Trappen, A. Martinez, D. Melanson, M. Yurtalan, Y. Tang, S. Novikov, J. Grover, S. Disseler, J. Basham, R. Das, D. Kim, A. Melville, B. Niedzielski, S. Weber, J. Yoder, D. Lidar, and A. Lupascu, Calibration of flux crosstalk in large-scale flux-tunable superconducting quantum circuits, *PRX Quantum* **2**, 040313 (2021).
- [68] A. M. van den Brink, A. J. Berkley, and M. Yalowsky, Mediated tunable coupling of flux qubits, *New Journal of Physics* **7**, 230 (2005).
- [69] X. Qiu, P. Zoller, and X. Li, Programmable quantum annealing architectures with ising quantum wires, *PRX Quantum* **1**, 020311 (2020).
- [70] Y. P. Zhong, H. S. Chang, K. J. Satzinger, M. H. Chou, A. Binfait, C. R. Conner, E. Dumur, J. Grebel, G. A. Peairs, R. G. Povey, D. I. Schuster, and A. N. Cleland, Violating bell's inequality with remotely connected superconducting qubits, *Nature Physics* **15**, 741 (2019).
- [71] P. Zhao, K. Linghu, Z. Li, P. Xu, R. Wang, G. Xue, Y. Jin, and H. Yu, Quantum crosstalk analysis for simultaneous gate operations on superconducting qubits, *PRX Quantum* **3**, 020301 (2022).
- [72] B. Kannan, M. J. Ruckriegel, D. L. Campbell, A. Frisk Kockum, J. Braumüller, D. K. Kim, M. Kjaergaard, P. Krantz, A. Melville, B. M. Niedzielski, A. Vepsäläinen, R. Winik, J. L. Yoder, F. Nori, T. P. Orlando, S. Gustavsson, and W. D. Oliver, Waveguide quantum electrodynamics with superconducting artificial giant atoms, *Nature* **583**, 775 (2020).
- [73] A. Schreiber, K. N. Cassemiro, V. Potoček, A. Gábris, I. Jex, and C. Silberhorn, Decoherence and disorder in quantum walks: From ballistic spread to localization, *Phys. Rev. Lett.* **106**, 180403 (2011).
- [74] D. A. Abanin, E. Altman, I. Bloch, and M. Serbyn, Colloquium: Many-body localization, thermalization, and entanglement, *Rev. Mod. Phys.* **91**, 021001 (2019).
- [75] A. C. Potter, R. Vasseur, and S. A. Parameswaran, Universal properties of many-body delocalization transitions, *Phys. Rev. X* **5**, 031033 (2015).

- [76] M. Serbyn, Z. Papić, and D. A. Abanin, Criterion for many-body localization-delocalization phase transition, *Phys. Rev. X* **5**, 041047 (2015).
- [77] B. Zeng, X. Chen, D.-L. Zhou, and X.-G. Wen, *Quantum Information Meets Quantum Matter* (Springer, New York, 2019).
- [78] D. J. Luitz, N. Laflorencie, and F. Alet, Many-body localization edge in the random-field heisenberg chain, *Phys. Rev. B* **91**, 081103 (2015).
- [79] R. Harris, J. Johansson, A. J. Berkley, M. W. Johnson, T. Lanting, S. Han, P. Bunyk, E. Ladizinsky, T. Oh, I. Perminov, E. Tolkacheva, S. Uchaikin, E. M. Chapple, C. Enderud, C. Rich, M. Thom, J. Wang, B. Wilson, and G. Rose, Experimental demonstration of a robust and scalable flux qubit, *Phys. Rev. B* **81**, 134510 (2010).
- [80] M. Orszag and J. Retamal, *Modern Challenges in Quantum Optics* (Springer, 2001).
- [81] V. Kendon and B. Tregenna, Decoherence can be useful in quantum walks, *Phys. Rev. A* **67**, 042315 (2003).